Available online at www.sciencedirect.com
ScienceDirect
Thin Solid Films 516 (2008) 7695–7700
www.elsevier.com/locate/tsf

# Size-dependent emission properties and intersubband transitions in cubic InN quantum dots and $In_xGa_{1-x}N$ clusters

Shih-Wei Feng *

*Department of Applied Physics, National University of Kaohsiung, No.700, Kaohsiung University Rd., Nan Tzu Dist., 811, Kaohsiung, Taiwan, ROC*

Received 16 October 2007; received in revised form 12 March 2008; accepted 18 March 2008
Available online 25 March 2008

**Abstract**

We theoretically studied size-dependent emission properties and intersubband (ISB) transitions in cubic InN (*c*-InN) quantum dots (QDs) and In-rich *c*-InGaN clusters. The quantum size effect can affect the energy levels and emission properties of such nano-structures, depending on composition, size, effective mass, and strain. In small *c*-InN QDs and In-rich *c*-InGaN clusters, strong quantum size effect enhances size-dependent emission properties and leads to fewer eigen-states. In larger *c*-InN QDs and In-rich InGaN clusters, ISB transitions between eigen-states of the conduction band can be applied in telecommunication devices. By varying the sizes of nano-structures, we can control the largest ISB transition energy difference between the ground state and the highest confined eigen-state. Simulation results also show that ISB absorption wavelengths can be altered by changing the composition and size of nano-structures.


*Keywords:* Quantum size effect; Intersubband (ISB) transition; Series expansion model; Cubic InGaN cluster; Cubic InN quantum dot

## 1. Introduction

InN has shown interesting physical properties such as small effective electron mass, large mobility, high saturation velocity, and small direct band gap in the nitride semiconductors [1–3]. InN quantum dots (QDs) and quantum wires have useful applications in optoelectronic devices. InN quantum dots (QDs) can be achieved by the Stranski–Krastanov growth mode and they generally exist in wurtzite structures (hexagonal, *h*-InN) as the thermodynamically stable phase [4–7]. By choosing proper substrates, cubic InN (*c*-InN) QDs can be grown [1–3,8]. Without large piezoelectric and spontaneous electric fields, the electronic properties of *c*-InN QDs are expected to be superior to those of *h*-InN QDs [1–3,8]. As was known, the dot size and shape can determine the energy levels and optical properties of *c*-InN QDs [4–7]. Similarly, carrier localization and size effect in In-rich *c*-InGaN clusters were proposed to explain the optical properties of *c*-InGaN/GaN heterostructures [9]. The optical properties and band structures of size-dependent *c*-InN QDs and *c*-InGaN clusters are still not clear.

On the other hand, the energy band gap of *c*-InN was found to be lower than that of *h*-InN [1–3]. Hence, *c*-InN QDs embedded in GaN or AlN show a larger confined potential and band offset. We can apply this advantage to develop intersubband (ISB) devices in tera-bit-rate telecommunication systems. However, the impact of the quantum size effect on the ISB transitions in *c*-InN QDs and In-rich *c*-InGaN clusters was not well studied.

In this study, to theoretically investigate size-dependent emission properties and ISB transitions in *c*-InN QDs and In-rich *c*-InGaN clusters, we calculate band structures of $In_xGa_{1-x}N$/GaN quantum cubes. The quantum size effect can affect the energy levels and emission properties of such nano-structures, depending on composition, size, effective mass, and strain. In small nano-structures, strong quantum size effect enhances size-dependent emission properties and leads to fewer eigen-states. In larger nano-structures, ISB transitions between eigen-states of the conduction band can be applicable in telecommunication devices. By varying the sizes of nano-structures, we can control the largest ISB transition energy difference between the ground state and the highest confined eigen-state. Simulation results also show that

* Tel.: +886 7 591 9470; fax: +886 7 591 9357.
*E-mail address:* swfeng@nuk.edu.tw.

0040-6090/$ - see front matter © 2008 Elsevier B.V. All rights reserved.
doi:10.1016/j.tsf.2008.03.025

ISB absorption wavelengths can be designed by changing the composition and size of nano-structures.

This paper is organized as follows: in Section 2, theoretical calculations of band structures of size- and composition-dependent $In_xGa_{1-x}N$/GaN quantum cubes are described. In Section 3, size-dependent emission properties of *c*-InN QDs and *c*-InGaN clusters will be discussed. In Section 4, impact of the quantum size effect on eigen-states and ISB transitions is reported. Finally, conclusions will be drawn in Section 5.

## 2. Band structures of size- and composition-dependent $In_xGa_{1-x}N$/GaN quantum cubes

InN and $In_xGa_{1-x}N$ quantum cubes, i.e. $L_x=L_y=L_z=L$, embedded in GaN matrixes were considered (Fig. 1(a)). A series expansion model was conducted to calculate the band structures of size- and composition-dependent $In_xGa_{1-x}N$ quantum cubes, as shown in Fig. 1(b). $E_n^c$, $E_n^{hh}$, and $E_n^{lh}$ ($n$=0, 1, 2, …) represent electron, heavy-hole, and light-hole $n$-th energy levels, respectively. $E_g$ is the material band gap of the $In_xGa_{1-x}N$ compound inside the quantum cube. We start with the Schrödinger equations [10,11]

$$\left\{-\frac{\hbar^2}{2}\left[\nabla_e\cdot\left(\frac{1}{m_e^*(\vec{r}_e)}\right)\nabla_e+\nabla_h\cdot\left(\frac{1}{m_h^*(\vec{r}_h)}\right)\nabla_h\right]+\frac{e^2}{4\pi\varepsilon|\vec{r}_e-\vec{r}_h|}+\Delta V_e(\vec{r}_e)+\Delta V_h(\vec{r}_h)\right\}\psi_{eh}(\vec{r}_e,\vec{r}_h)=E\psi_{eh}(\vec{r}_e,\vec{r}_h) \quad (1)$$

Here, $M_e^*(\vec{r}_e)$ and $M_h^*(\vec{r}_h)$ represent the effective masses of electron and holes, respectively. $\Delta V_e(\vec{r}_e)$ and $\Delta V_h(\vec{r}_h)$ are the spatial distributions of potential for electrons and holes, respectively. $E$ and $\psi_{eh}(\vec{r}_e,\vec{r}_h)$ are the eigen-energy and the corresponding wave function of the system, respectively. The term $\frac{e^2}{4\pi\varepsilon|\vec{r}_e-\vec{r}_h|}$ describes the electron-hole Coulomb interaction.

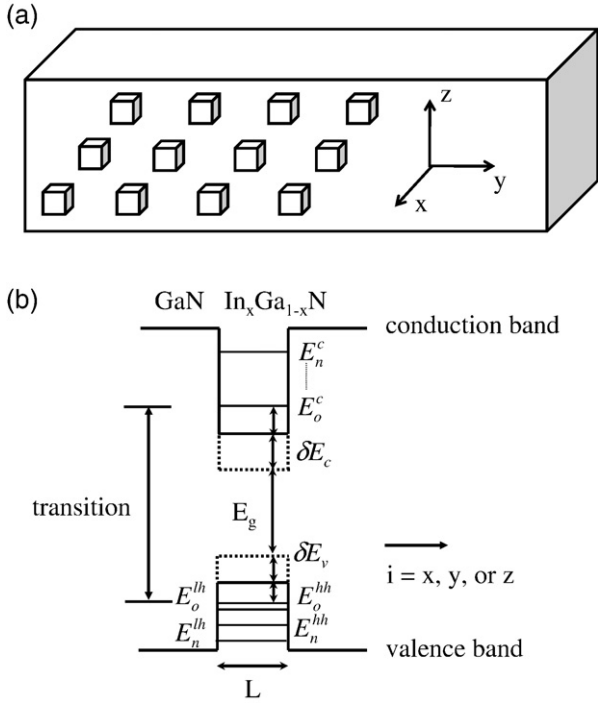


Fig. 1. (a) Schematic diagram of cubic InN and/or $In_xGa_{1-x}N$ quantum cubes embedded in GaN matrix. (b) Schematic band structures of a quantum cube with size $L$.

It has been reported that the increase of effective band gap in energy discretization is more important than the enhancement of exciton binding energy in calculating the effective band gap of a QD [12]. Hence, it is reasonable to express the exciton wave function $\psi_{eh}(\vec{r}_e,\vec{r}_h)$ as the product of electron and hole wavefunctions.

$$\psi_{eh}(\vec{r}_e,\vec{r}_h)=\psi_e(\vec{r}_e)\psi_h(\vec{r}_h) \quad (2)$$

Here $\psi_e(\vec{r}_e)$ and $\psi_h(\vec{r}_h)$ stand for the wave functions of electron and hole, respectively. Then, the equation for electron and hole wave functions can be decoupled as

$$\left[-\frac{\hbar^2}{2}\nabla_e\cdot\left(\frac{1}{m_e^*(\vec{r}_e)}\right)\nabla_e+\Delta V_e(\vec{r}_e)\right]\psi_e(\vec{r}_e)=E_e\psi_e(\vec{r}_e) \quad (3a)$$

$$\left[-\frac{\hbar^2}{2}\nabla_h\cdot\left(\frac{1}{m_h^*(\vec{r}_h)}\right)\nabla_h+\Delta V_h(\vec{r}_h)\right]\psi_h(\vec{r}_h)=E_h\psi_h(\vec{r}_h) \quad (3b)$$

with

$$E_e+E_h=E \quad (3c)$$

The solutions of Eq. (3a) and (3b) can be expressed as the series expansions of the ortho-normal functions $\varphi_{l_e,m_e,n_e}$ and $\varphi_{l_h,m_h,n_h}$, which form complete sets, respectively, with properly chosen coefficients, $d_{l_e,m_e,n_e}$ and $d_{l_h,m_h,n_h}$, as follows:

$$\psi_e(\vec{r}_e)=\sum_{l_e,m_e,n_e} d_{l_e,m_e,n_e}\varphi_{l_e,m_e,n_e}(x,y,z) \quad (4a)$$

$$\psi_h(\vec{r}_h)=\sum_{l_h,m_h,n_h} d_{l_h,m_h,n_h}\varphi_{l_h,m_h,n_h}(x,y,z) \quad (4b)$$

The functions $\varphi_{l_e,m_e,n_e}(x,y,z)$ and $\varphi_{l_h,m_h,n_h}(x,y,z)$ are given by

$$\varphi_{l_e,m_e,n_e}(x,y,z)=\sqrt{\frac{8}{L_xL_yL_z}}\sin\left[l_e\pi\left(\frac{1}{2}-\frac{x}{L_x}\right)\right]\times\sin\left[m_e\pi\left(\frac{1}{2}-\frac{y}{L_y}\right)\right]\sin\left[n_e\pi\left(\frac{1}{2}-\frac{z}{L_z}\right)\right] \quad (5a)$$

$$\varphi_{l_h,m_h,n_h}(x,y,z)=\sqrt{\frac{8}{L_xL_yL_z}}\sin\left[l_h\pi\left(\frac{1}{2}-\frac{x}{L_x}\right)\right]\times\sin\left[m_h\pi\left(\frac{1}{2}-\frac{y}{L_y}\right)\right]\sin\left[n_h\pi\left(\frac{1}{2}-\frac{z}{L_z}\right)\right] \quad (5b)$$

Here, $L_x$, $L_y$, and $L_z$ represent the dimensions of the quantum box. Also, the positive integers $l_{e(h)}$, $m_{e(h)}$, and $n_{e(h)}$ form the set of quantum numbers denoting the discrete states in the conduction (valence) band. The functions $\varphi l_e,m_e,n_e$ $(x,y,z)$ and

$\varphi l_h,m_h,n_h$ $(x,y,z)$ are actually the eigen-functions of the discrete states in the quantum box with the assumption that the barrier potential is infinitely high. In the model, the real wave functions of the discrete states, $\psi_e(\vec{r_e})$ and $\psi_h(\vec{r_h})$, in the quantum box of a finite barrier potential height are series-expanded based on the ortho-normal complete set shown in Eqs. (5a) and (5b). The eigen-functions of infinite-potential barrier for the discrete wave functions are slightly modified. In the real case, wave functions extend into the barrier to a certain distance. Following the empirical conclusion, the penetration length was supposed to be equal to the quantum cube dimension [10,11].

After substituting Eqs. (4a), (4b), (5a), and (5b) into Eqs. (3a) and (3b), we then multiplied both sides of Eqs. (3a) and (3b) by $\varphi l'_i,m'_i,n'_i$ $(x,y,z)(i=e,h)$ and integrated over the quantum box region (with extended dimensions). Such procedures lead to the following matrix eigen-problem as

$$\sum\left(A_{l_im_in_il'_im'_in'_i}\right)-E\delta_{l_il'_i}\delta_{m_im'_i}\delta_{n_in'_i})d_{l'_im'_in'_i}=0 \tag{6}$$

The matrix elements are given by

$$\begin{aligned}A_{l_im_in_il'_im'_in'_i}=&\left[\frac{\hbar^2\pi^2}{2}\cdot\frac{1}{m^*_{iB}}\cdot\left(\frac{l_il'_i}{L_x^2}+\frac{m_im'_i}{L_y^2}+\frac{n_in'_i}{L_z^2}\right)+(E_{iB}-E_{iW})\right]\\&\times\delta_{l_il'_i}\delta_{m_im'_i}\delta_{n_in'_i}+\int\int\int\left[\frac{\hbar^2}{2}\left(\frac{1}{m^*_{iC}}-\frac{1}{m^*_{iB}}\right)\right.\\&\times(\varphi'_{l_im_in_ix}\varphi'_{l'_im'_in'_ix}+\varphi'_{l_im_in_iy}\varphi'_{l'_im'_in'_iy}\\&\left.+\varphi'_{l_im_in_iz}\varphi'_{l'_im'_in'_iz})-(E_{iB}-E_{iC})\varphi_{l_im_in_i}\varphi_{l'_im'_in'_i}\right]dxdydz\\&i=e,h\end{aligned} \tag{7}$$

Here, $\varphi'_{l_im_in_ix}=\frac{d\varphi_{l_im_in_i}}{dx}$, $\varphi'_{l_im_in_iy}=\frac{d\varphi_{l_im_in_i}}{dy}$, and $\varphi'_{l_im_in_iz}=\frac{d\varphi_{l_im_in_i}}{dz}$. $m^*_{iC}$ and $m^*_{iB}$ are the effective masses within and outside the quantum box, respectively. $E_{iC}$ and $E_{iB}$ are the potential heights within and outside the box, respectively. Eq. (7) is then solved numerically by considering $l_e$, $m_e$, $n_e$, $l_h$, $m_h$, and $n_h$ up to 10.

The band structure of a low-dimension system can be altered by strain. In general, with compressive strain in the quantum-confined region, the conduction-band and valence-band edges are shifted upward and downward, respectively. The strain-induced band structure modification of a quantum dot system can be expressed as a product of strain components and a deformation potential [12]. For hydrostatic strains, the strain effects of the conduction bands are decoupled from those of the valence bands. In the following, we assume that strain is zero outside the quantum cube and is compressed inside, as depicted in Fig. 1(b). In this situation, at the $\Gamma$ point ($k=0$), the conduction band edge is modified by the energy shift $\delta E_H^C$ as

$$\delta E_H^c=a_c\left(\varepsilon_{xx}+\varepsilon_{yy}+\varepsilon_{zz}\right)=a_cI \tag{8}$$

with

$$I=\varepsilon_{xx}+\varepsilon_{yy}+\varepsilon_{zz} \tag{9}$$

Here, $a_c$ is the hydrostatic deformation potential of the conduction band. $\varepsilon_{xx}$, $\varepsilon_{yy}$, and $\varepsilon_{zz}$ represent the strains in the $x$, $y$, and $z$ directions, respectively. $I$ is the isotropic strain and can be approximated by [12]:

$$I=2\varepsilon_0\frac{1-2v}{1-v} \tag{10}$$

Here, $v$ is the Poisson ratio. For many semiconductors, the Poisson ratio is close to 1/3. $\varepsilon_0$ expresses the relative lattice constant mismatch of inner and outer materials.

Also, the valence band edge is modified by the energy shift $\delta E_H^v$ as

$$\delta E_H^v=a_v\left(\varepsilon_{xx}+\varepsilon_{yy}+\varepsilon_{zz}\right)=a_vI \tag{11}$$

Here, $a_v$ is the hydrostatic deformation potential of the valence band. Hence, with the hydrostatic strain, the band gap is modified by the total hydrostatic deformation potential $a$ with $a=a_c+a_v$. After certain arrangements, an eigen-valued problem of a $10\times10\times10$ tensor for either conduction or valence band is solved.

Table 1 lists the physical parameters used in our calculations [13,14]. The material band-gap energy $E_g(x)$ for $c$-$In_xGa_{1-x}N$ with a bowing constant $b=1.4$ eV is expressed as [13,14]

$$E_g(x)=0.78x+3.299(1-x)-1.4x(1-x) \tag{12}$$

Except for the band gap energy, the physical parameters of $c$-$In_xGa_{1-x}N$ can be expressed as the linear interpolation formula of InN and GaN.

$$P(In_xGa_{1-x}N)=xP(InN)+(1-x)P(GaN) \tag{13}$$

Here, $P$ represents any material parameter, such as effective mass. The band offset ratio for the conduction and valence bands is assumed to be 0.65:0.35 [15]. The transition energy $E^c_{hh}$ ($E^c_{lh}$) between the ground electron state and ground heavy-hole (light-hole) state is defined as

$$E^c_{hh}\left(E^c_{lh}\right)\equiv E^c_0+\delta E_c+E_g+\delta E_v+E^{hh}_0\left(E^{lh}_0\right) \tag{14}$$

## 3. Size-dependent optical properties of *c*-InN QDs and *c*-InGaN clusters

Fig. 2(a) shows the transition energy $E^c_{hh}$ between the ground electron state and ground heavy-hole state. The curve represents the material band gap $E_g(x)$ of cubic $In_xGa_{1-x}N$. Simulation results show that the size and composition of InGaN nano-structures can affect their emission properties. In In-rich InGaN clusters, the size variations of $E^c_{hh}$ and the energy difference between $E^c_{hh}$ and $E_g(x)$ become apparent. These imply that quantum size effect becomes dominant in determining the optical properties of smaller InGaN nano-structures. This result can provide evidence for the debate about the bandgap of InN QDs as well as In-rich InGaN clusters. For luminescence measurements, experimental results are the statistics of the InGaN clusters with various sizes and compositions. For comparison, the reported PL peak position (○) of the In-rich phase versus In composition $x=0.56$ in cubic GaN/InGaN heterostructures was plotted [9]. We speculate that

Table 1
Material parameters of GaN and InN used for calculations [13,14]

| | GaN | InN |
|---|---|---|
| Lattice constant $a$ (Å) | 4.5 | 4.98 |
| $E_g^{\Gamma}$(eV) | 3.299 | 0.78 |
| Effective mass ($m_0$) | | |
| Electron | 0.15 | 0.07 |
| Heavy hole along $c$-axis $m_{hh//}$ | 0.847 | 0.806 |
| Perpendicular to $c$-axis $m_{hh\perp}$ | 1.526 | 1.55 |
| Heavy hole $m_{hh}=(m_{hh\perp}^2\, m_{hh//})^{1/3}$ | | |
| Light hole along $c$-axis $m_{lh//}$ | 0.236 | 0.159 |
| Perpendicular to $c$-axis $m_{lh\perp}$ | 0.105 | 0.07 |
| Light hole $m_{lh}=(m_{lh\perp}^2\, m_{lh//})^{1/3}$ | | |
| Momentum matrix element $E_p$(eV) | 25 | 17.2 |
| Hydrostatic deformation potential (eV) | | |
| Conduction band $a_c$ | −6.71 | −2.65 |
| Valence band $a_v$ | −0.69 | −0.7 |

the distribution of QD sizes is 4–6 nm. This is generally consistent with InGaN cluster sizes in our previous transmission electron microscopy pictures [16,17]. Furthermore, simulation results also reveal that the optical properties of InGaN clusters depend on the important factors of composition, cluster size, effective mass, and strain. Fig. 2(b) shows the transition energy $E_{lh}^c$ between the ground electron state and ground light-hole state. Compared with $E_{hh}^c$, $E_{lh}^c$ show larger size variations, higher electron transition energies, and fewer transitions. These are attributed to the enhanced quantum size effect of light-holes.

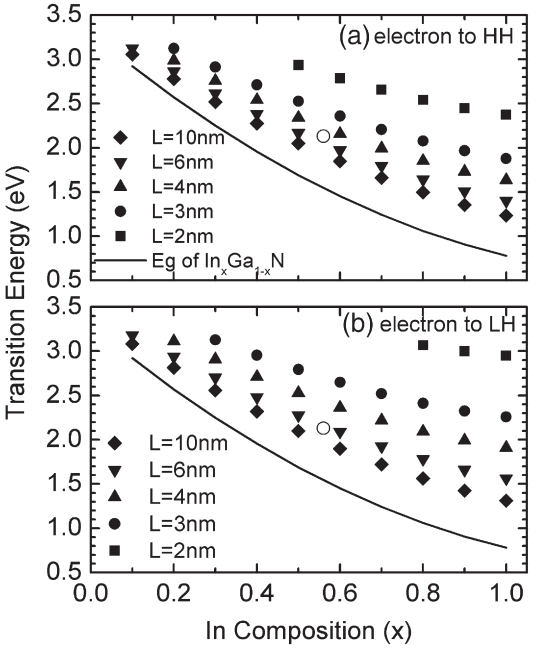


Fig. 2. (a) Transition energy $E_{hh}^c$ between electron and heavy-hole ground-states as functions of indium composition. For comparison, the reported PL peak position of the In-rich phase with In composition $x=0.56$ in GaN/InGaN heterostructures was marked as empty circle (○) [11]. (b) Transition energy $E_{lh}^c$ between electron and light-hole ground-states as functions of indium composition.

## 4. Impact of the quantum-size effect on eigen-energies and ISB transitions

To investigate the quantum-size effect on electronic states, the electron, heavy-hole, and light-hole eigen-energies were studied. Fig. 3(a), (b), and (c) show electron ($E_n^c$) eigen-energies for cube sizes $L=3$ nm, $L=5$ nm, and $L=10$ nm, respectively. With the same composition of the cube, some phenomena for smaller cubes were observed:

(a) the ground state shifts upward;
(b) the largest ISB transition energy, $E_{\mathrm{ISB}}^{\max}$, between the ground eigen-state and the highest confined eigen-state become smaller;
(c) the number of eigen-states is decreased;
(d) eigen-energies are discrete.

These are attributed to the enhanced quantum confinement effect in small cubes. Also, because of the lighter effective mass of InN, the features show that the quantum-size effect could affect the electronic states of smaller In-rich InGaN clusters. The smaller number of eigen-states in smaller In-rich InGaN clusters also implies that ISB transitions between electron eigen-states may be inefficient. The details will be discussed later in this article.

Fig. 4 shows heavy-hole eigen-energy ($E_n^{hh}$) for cube sizes (a)$L=3$ nm, (b)$L=5$ nm, and (c)$L=10$ nm. Because the larger effective mass of heavy-hole results in a weaker quantum-confinement effect, there is greater density of states (DOS) of $E_n^{hh}$ and ground states $E_0^{hh}$ are near the band edge. Also, due to a high degeneration of $E_n^{hh}$ in cubes with size $L=10$ nm, the

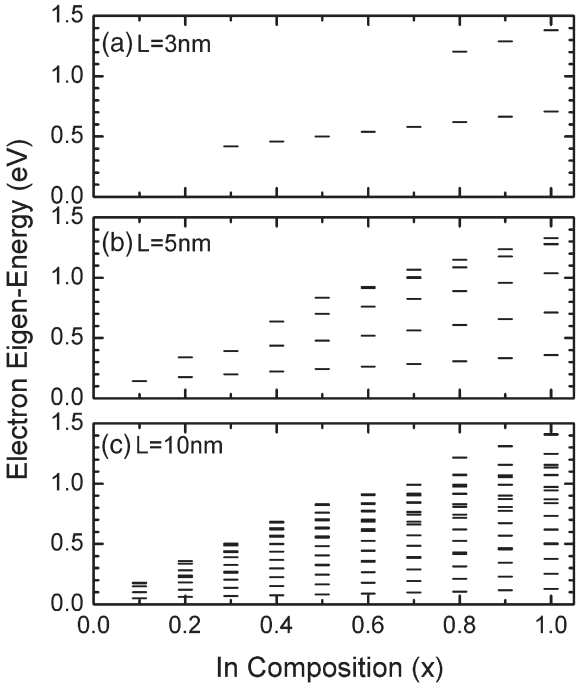


Fig. 3. Electron eigen-energy ($E_h^c$) as functions of indium composition for quantum cube sizes (a) $L=3$ nm, (b) $L=5$ nm, and (c) $L=10$ nm.

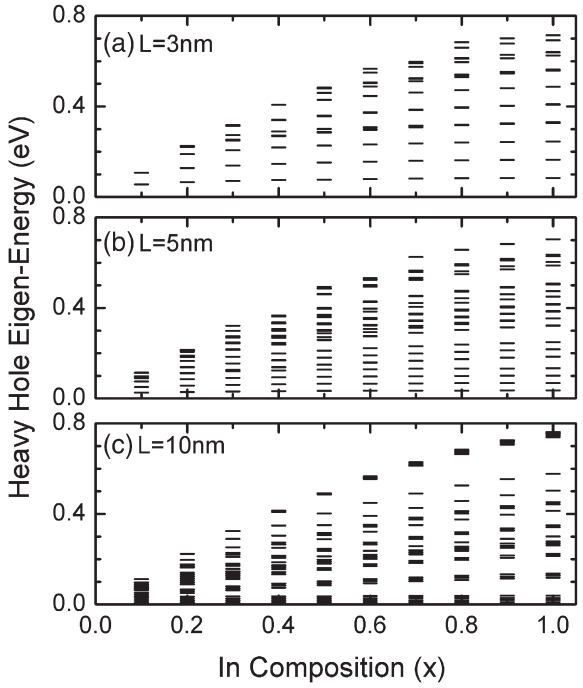


Fig. 4. Heavy-hole eigen-energy ($E_n^{hh}$) as functions of indium composition for quantum cube sizes (a) $L=3$ nm, (b) $L=5$ nm, and (c) $L=10$ nm.

number of $E_n^{hh}$ seems to decrease. The trends indicate that holes can be easily populated in the eigen-states and act as acceptors to emit photons. It was reported that strong hole localization of the valence states occurs along the [110] In–N–In–N chains in cubic InGaN alloys [18]. The positron annihilation measurement also shows that hole localizations in atomic In–N chains form localization excitons to emit the light [19]. Our simulation results are consistent with the previous argument. Meanwhile, the eigen-states of light-hole in Fig. 5 are discrete. This also shows that the effective mass and the quantum-confinement effect play important roles in determining the electronic structures of the QDs. Because of the discrete $E_n^{lh}$, emission lights by the transitions from electron to heavy-hole eigen-states are dominant. Furthermore, the valence band mixing effect describes the coupling effect between the heavy-hole and light-hole bands [20]. Because the light-hole eigen-states in smaller quantum cubes were few and the eigen-energies are not near the band-edge, the coupling effect between heavy-hole and light-hole bands should be negligible. The results support our numerical hypothesis.

Fig. 6(a), (b), and (c) summarize the numbers of confined electron, heavy-hole, and light-hole eigen-states, respectively. As the indium composition increases, the larger quantum confinement potential confines more bound-states. Hence, the number of eigen-states increases. In both conduction and valence bands, large size variations of $E_n^c$, $E_n^{hh}$, and $E_n^{lh}$ imply that the quantum confinement effect is a critical factor in determining the electronic states of InGaN clusters. Low DOS in smaller cubes implies that ISB transitions in smaller QDs or InGaN clusters may be inefficient. Also, compared with $E_n^{hh}$, lower DOSs and larger size variations of $E_n^{lh}$ can also be explained by the enhanced quantum confinement effect.

Fig. 7 shows the largest ISB transition energy, $E_{\mathrm{ISB}}^{\max}$, between the ground state and the highest confined eigen-state for (a) electron, (b) heavy-hole, and (c) light-hole. In In-rich InGaN quantum cubes, the larger confined potential of the conduction

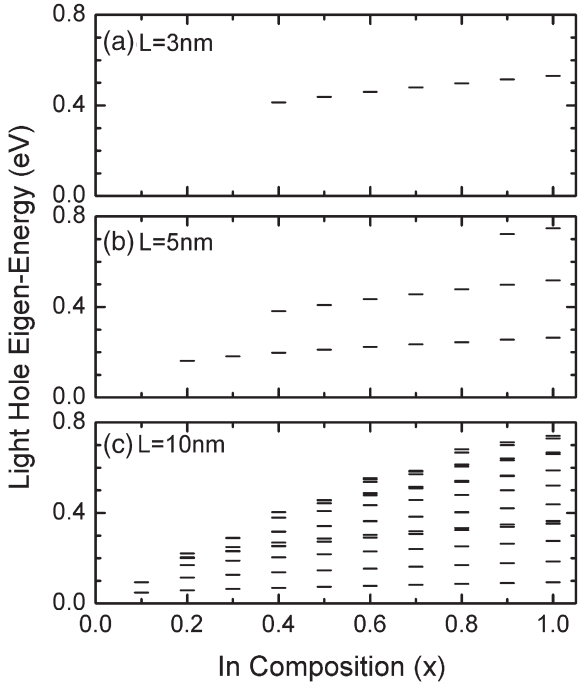


Fig. 5. Light-hole eigen-energy ($E_n^{lh}$) as functions of indium composition for quantum cube sizes (a) $L=3$ nm, (b) $L=5$ nm, and (c) $L=10$ nm.

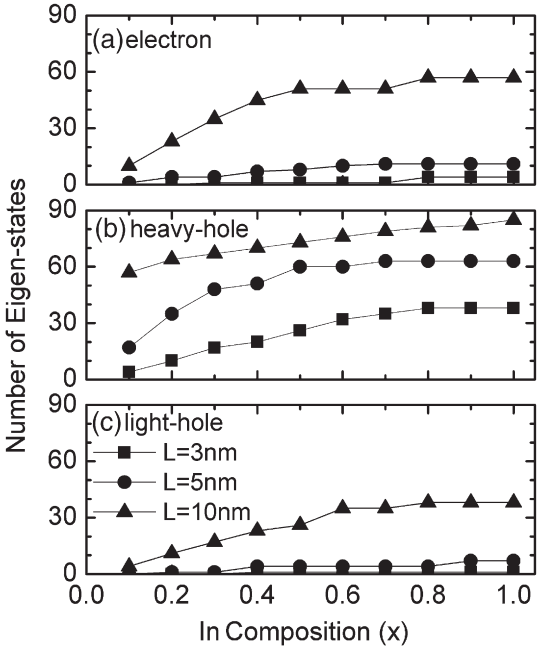


Fig. 6. Numbers of (a) electron, (b) heavy-hole, and (c) light-hole eigen-states as functions of indium composition for cube sizes $L=3$ nm, $L=5$ nm, and $L=10$ nm.

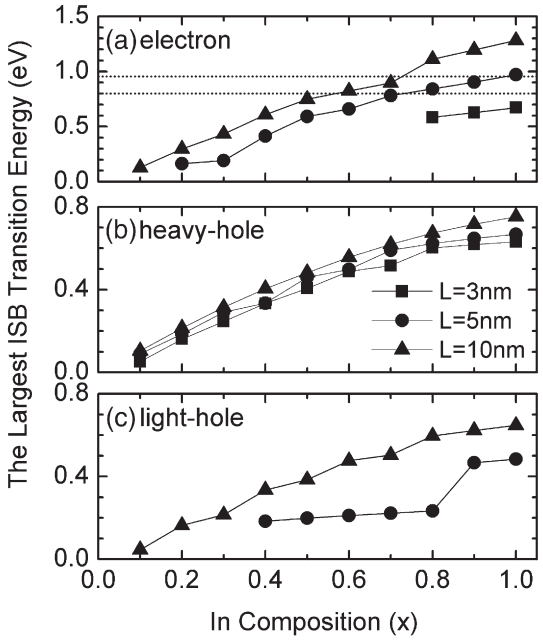


Fig. 7. The largest ISB transition energies $E_{ISB}^{max}$ of (a) electron, (b) heavy-hole, and (c) light-hole as functions of indium composition for cube sizes $L=3$ nm, $L=5$ nm, and $L=10$ nm.

band results in an increase of $E_{ISB}^{max}$. Due to the enhanced quantum-size effect, $E_{ISB}^{max}$ of In-rich InGaN quantum cubes are more sensitive to size than those of low indium ones. Also, the energies between two dot lines represent the telecommunication window around 0.800–0.953 eV (1.55 μm–1.3 μm). Simulation results suggest that ISB transitions in the conduction of In-rich InGaN clusters are useful for telecommunication devices. By controlling the quantum-confinement effect, one can determine $E_{ISB}^{max}$. Meanwhile, the small quantum confined potential of the valence band implies that ISB transitions between hole eigenstates are suitable for detector applications. $E_{ISB}^{max}$ of light-hole are smaller than those of heavy-hole and they show larger size variations. The results also show that the effective mass and the quantum-confinement effect can determine the band structures of the In-rich InGaN clusters. By changing the composition and size of clusters, one can design detectors of the desired absorptions wavelengths.

## 5. Conclusions

In summary, we have theoretically studied size-dependent emission properties and ISB transitions in *c*-InN and *c*-InGaN nano-structures. The composition, size, effective mass, and strain of such nano-structures can affect their energy levels and emission properties. In small nano-structures, strong quantum size effect enhances size-dependent emission properties. Simulation results show larger nano-structures can be used to develop ISB telecommunication devices. By varying the sizes of nano-structures, we can control the largest ISB transition energy and ISB absorption wavelengths. The presented results show that cubic III-nitride nano-structures are suitable for developing telecommunications and photovoltaic devices.

## Acknowledgments

This research was supported by the National Science Council, Republic of China, under grants NSC 95-2112-M-390-005 and NSC 96-2918-I-390-002.

## References

[1] S.K. O'Leary, B.E. Foutz, M.S. Shur, L.F. Eastman, Appl. Phys. Lett. 88 (2006) 152113.
[2] J. Schörmann, D.J. As, K. Lischka, P. Schley, R. Goldhahn, S.F. Li, W. Löffler, M. Hetterich, H. Kalt, Appl. Phys. Lett. 89 (2006) 261903.
[3] J.G. Lozano, F.M. Morales, R. García, D. González, V. Lebedev, Ch.Y. Wang, V. Cimalla, O. Ambacher, Appl. Phys. Lett. 90 (2007) 91901.
[4] I.K. Park, M.K. Kwon, S.H. Baek, Y.W. Ok, T.Y. Seong, S.J. Parka, Y.S. Kim, Y.T. Moon, D.J. Kim, Appl. Phys. Lett. 87 (2005) 061906.
[5] J.G. Lozano, A.M. Sánchez, R. García, D. Gonzalez, O. Briot, S. Ruffenach, Appl. Phys. Lett. 88 (2006) 51913.
[6] A. Yoshikawa, N. Hashimoto, N. Kikukawa, S.B. Che, Y. Ishitani, Appl. Phys. Lett. 86 (2005) 153115.
[7] W.C. Ke, C.P. Fu, C.Y. Chen, L. Lee, C.S. Ku, W.C. Chou, W.H. Chang, M.C. Lee, W.K. Chen, W.J. Lin, Y.C. Cheng, Appl. Phys. Lett. 86 (2005) 191913.
[8] D. Bagayoko, L. Franklin, G.L. Zhao, J. Appl. Phys. 96 (2004) 4297.
[9] O. Husberg, A. Khartchenko, D.J. As, H. Vogelsang, T. Frey, D. Schikora, K. Lischka, O.C. Noriega, A. Tabata, J.R. Leite, Appl. Phys. Lett. 79 (2001) 1243.
[10] H. Gotoh, H. Ando, T. Takagahara, J. Appl. Phys. 81 (1997) 1785.
[11] S. Gangopadhyay, B.R. Nag, Nanotechnology 8 (1997) 14.
[12] D. Bimberg, M. Grundmann, N.N. Ledentsov, Quantum Dot Heterostructures, John Wiely & Sons, England, 1999.
[13] I. Vurgaftman, J.R. Meyer, J. Appl. Phys. 94 (2003) 3675.
[14] T. Suzuki, H. Yaguchi, H. Okumura, Y. Ishida, S. Yoshida, Jpn. J. Appl. Phys. 39 (2000) L497.
[15] D.R. Hang, C.H. Chen, Y.F. Chen, H.X. Jiang, J.Y. Lin, J. Appl. Phys. 90 (2001) 1887.
[16] S.W. Feng, E.C. Lin, T.Y. Tang, Y.C. Cheng, H.C. Wang, C.C. Yang, K.J. Ma, C.H. Shen, L.C. Chen, K.H. Kim, J.Y. Lin, H.X. Jiang, Appl. Phys. Lett. 83 (2003) 3906.
[17] S.W. Feng, T.Y. Tang, Y.C. Lu, S.J. Liu, E.C. Lin, C.C. Yang, K.J. Ma, C.H. Shen, L.C. Chen, K.H. Kim, J.Y. Lin, H.X. Jiang, J. Appl. Phys. 95 (2004) 5388.
[18] S.H. Park, Appl. Phys. Lett. 80 (2002) 2830.
[19] S.F. Chichibu, A. Uedono, T. Onuma, B.A. Haskell, A. Chakraborty, T. Koyama, P.T. Feni, S. Keller, S.P. Denbaars, J.S. Speck, U.K. Mishra, S. Nakamura, S. Yamaguchi, S. Kamiyama, H. Amano, I. Akasaki, J. Han, T. Sota, Nat. Matters 5 (2006) 810.
[20] P.R.C. Kent, A. Zunger, Appl. Phys. Lett. 79 (2001) 1977.